LBL-26562
Preprint

Lawrence Berkeley Laboratory
UNIVERSITY OF CALIFORNIA

Submitted to International Journal of Radiation Oncology, Biology, Physics

Comparison of Different Radiation Types and Irradiation Geometries in Stereotactic Radiosurgery

M.H. Phillips, K.A. Frankel, J.T. Lyman, J.I. Fabrikant, and R.P. Levy

January 1989

Donner Laboratory

Biology & Medicine Division

Prepared for the U.S. Department of Energy under Contract Number DE-AC03-76SF00098.

DISCLAIMER

COMPARISON OF DIFFERENT RADIATION TYPES AND IRRADIATION GEOMETRIES IN STEREOTACTIC RADIOSURGERY[1]

Mark H. Phillips
Kenneth A. Frankel
John T. Lyman
Jacob I. Fabrikant
Richard P. Levy.

Research Medicine and Radiation Biophysics Division,
Lawrence Berkeley Laboratory,
1 Cyclotron Road,
Berkeley, CA 94720

[1]This research was supported by the Office of Health and Environmental Research, U.S. Department of Energy Contract DE-AC03-76SF00098.

Abstract

Recent interest in stereotactic radiosurgery of intracranial lesions, and the development of stereotactic irradiation techniques has led to the need for a systematic and complete comparison of these methods. A method for conducting these comparisons is proposed and is applied to a set of currently-used stereotactic radiosurgical techniques. 3-dimensional treatment planning calculations are used to compare dose distributions for several different radiation types and irradiation geometries. Calculations were performed using charged particles (H, He, C, and Ne ions) and the irradiation geometry currently used at Lawrence Berkeley Laboratory. Photons in the Gamma Knife configuration and the Heidelberg Linac arc method are used. The 3-dimensional dose distributions were evaluated by means of dose-volume histograms and integral doses to the target volume and to normal brain. The effects of target volume, shape and location are studied. The charged particle dose distributions are more favorable than those of the photon methods. The differences between charged particles and photons increases with increasing target volume. The differences between different charged particle species are small, as are the effects of target shape and location.

Key Words: stereotactic radiosurgery, charged particles, photons, AVM, dose comparison

INTRODUCTION

There has been a recent surge in interest in stereotactic radiosurgery of intracranial lesions, such as arteriovenous malformations (AVMs), tumors and isolated metastases [3,4,6,7,9,11,12,13]. Much experience has been gained at a number of medical centers around the world in the past three decades [1,4,6,8,12,13]. The successful treatment of tumors and AVMs that were surgically-inaccessible has spawned the dissemination of stereotactic radiosurgical techniques at a number of different institutions. Each of these institutions has developed a unique radiosurgical procedure, using a range of radiation types and irradiation geometries.

The essential component of the stereotactic radiosurgical procedure is the delivery of a dose of radiation that is tightly confined to the region of pathological tissue. Unlike conventional radiotherapy which utilizes a number of therapeutic strategies in addition to dose localization and which delivers small daily doses over many fractions, stereotactic radiosurgery relies on precise dose localization to deliver one or two large fractions of radiation to cause damage to tissue within the target volume while sparing adjacent, normal tissue. The exact means by which these tightly-confined dose distributions are achieved vary depending on the radiation source, but all rely on stereotactic localization techniques to guide a number of well-defined beams of radiation that are isocentrically arranged about the center of the target volume.

The efficacy of one type of radiation or irradiation scheme over another is not yet clinically established. Differences between treatment centers in patient selection criteria, treatment volumes and margins, and in definitions of cures and complications make such clinical comparisons difficult. In addition, the physiological and biological characteristics of arteriovenous malformations that are important factors in determining the precise radiosurgical treatment parameters are not completely understood or are impossible to visualize by radiological studies. These character-

istics include the volume of flow through the AVM, the extent, size and distribution of arterial feeding and venous draining vessels, differences in radiosensitivity between the various compartments of the AVM and nearby normal tissue (neural and vascular), and the effects of hemodynamic changes on the AVM and on normal brain.

The recent interest in stereotactic radiosurgical techniques and the proliferation of medical centers using such techniques makes it more necessary than ever that a basis for comparisons be found, and that such comparisons be made. The first step is to compare the different radiation types and irradiation geometries on the basis of dose distributions. 1-dimensional dose profiles and 2-dimensional isodose contours are the most common means used to make such comparisons. However, they are limited in their characterization of the dose delivered to volumes of tissue, and do not give a complete picture of the situation. We use dose-volume histograms, calculated from dose matrices generated by a 3-dimensional, CT-based treatment planning program to present a very complete picture of the distribution of radiation within any given volume of tissue. An optimal treatment modality delivers a uniform dose throughout the target volume while minimizing the dose to surrounding, healthy tissue. Dose-volume histograms provide the best means to evaluate treatment modalities based on these criteria.

Using these methods, we have calculated dose-volume histograms for several representative radiosurgical techniques–the helium-ion technique used at Lawrence Berkeley Laboratory (LBL) [10], the Gamma Knife in Sweden [3], and the LINAC technique used at Heidelberg [5]. A range of targets were chosen to explore the impact of lesion size, shape and position on the distribution of radiation to the target volume and to regions of normal tissue. Volumes of normal tissue were circumscribed in order to assess the radiation burden to various adjacent critical healthy tissues.

METHOD

The 3-dimensional treatment planning program, written at LBL, calculates dose distributions on a set of CT images spanning the entire head. The program, written in FORTRAN, takes 20 min to 8 hr of CPU time on a VAX 11/780 or microVAX (Digital Equipment Corp., Maynard, MA) depending on the number and size of the beamports. The calculations were performed on a grid 3.1 x 3.1 x 3 mm (0.029 cm^3). The beamport parameters (number, orientation, weighting and degree of compensation) are input by means of a setup file. The program outputs files containing the dose distribution on each CT slice. The program automatically matches the shape of the beamport collimator to the projection of the target volume in the direction of the beamport. The dimensions of the apertures are set in order to place the 90% isodose contour at the edge of the target volume. Charged-particle compensation and ranges are automatically calculated to place the distal edge of the Bragg peak on the distal edge of the target contour. Values of the spread-out Bragg peak are chosen by the computer in 1 cm increments to conform to the dimension of the target along the beamport direction.

Target volumes were selected to provide a range of sizes, shapes, and locations. One set of volumes was selected from actual cases of AVMs treated at LBL in order to provide realistic target shapes and sizes. Six cases were chosen to fit into six categories defined by size and location: small, medium or large, and centrally or peripherally located. The size categories are: (a) small is less than 4 cm^3, corresponding to a diameter of less than 2 cm for a spherical volume, (b) medium is a volume greater 4 cm^3 and less than 14 cm^3, equivalent to a diameter from 2 to 3 cm for a spherical volume, and (c) large is greater than 14 cm^3, or a diameter greater than 3 cm. Centrally located lesions were chosen as falling near or within the thalamus; peripheral lesions were located near or adjacent to the skull.

Another set of targets was used in order to have an easily reproducible stan-

dard of comparison. This set consisted of spherical targets located in the center of the brain, which corresponds to a position located on the midline of the brain, approximately 3 cm above the level of the sella turcica, and midway between the posterior and anterior extent of the skull. The targets were 1, 2, 3, 4, and 5 cm in diameter, corresponding to volumes of 0.5, 4.1, 14, 33, and 65 cm^3, respectively.

The dose to normal tissue was assessed by defining a series of volumes. These volumes were (a) the entire brain, exclusive of the target volume, (b) a particular functional region of interest, such as the brainstem, which lay outside the target volume, and (c) constant-thickness shells of tissue that surrounded the target volume and were defined by contours that lay a given distance, e.g. 1 cm, from the boundaries of the target volume.

The radiation types were divided into charged particles and photons. The charged particles used were protons, helium ions, carbon ions, and neon ions. The photons were from an 8-MV linear accelerator. Depth-dose curves for these radiations are presented in Figure 1. The charged particle distributions are isoeffect curves, where the physical dose distributions have meen multiplied by LET-dependent RBE values to provide a region of constant cell survival in the spread Bragg peak region. The depth-dose curve for the 8-MV photons is for a 10 x 10 cm field, and no adjustment was made for different size fields. Dose fall-off lateral to the beam direction was accounted for in all cases.

Irradiation geometries were defined by number of beamports, their spatial orientation, and their weighting. The charged particle irradiation geometry for each treatment plan was determined by the techniques developed and used in the clinical research program at LBL. For small to medium lesions, this typically consisted of four beams, all from one side of the head, two beams in the coronal plane and two in the axial. Each beam is 20-30° from the lateral direction. For lesions falling exactly on midline, such as for the spherical targets described above, four beams

lying in the axial plane were used, two each from the left and right sides of the head, and 20-30° from the lateral direction. For large target volumes not located on the midline, a combination of four beams were used; they were from the anterior, posterior and lateral directions and were confined to the affected side of the head

Two photon irradiation geometries were used–that of the Gamma Knife with 179 beams [3], and that of the isocentrically-mounted Linac as used in Heidelberg [5]. In order to speed computation time, the 179 beams of the Gamma Knife were often approximated by either 54 or 99 beams after tests were conducted to determine that these approximations did not significantly alter the dose-volume histograms and integral doses. The continuous arcs of the Linac method were approximated by 55 beams. In both of these cases, the angular orientations of the beamports used were taken from the published reports, and the diminished number of ports used was achieved by deleting some symmetrically-distributed subset of those. In both the charged particle and photon treatment plans, all beamports were weighted equally.

Dose-volume histograms were calculated using the set of dose distribution files calculated for each CT slice. Histograms could be calculated for any volume defined by a set of contours and for the difference in volume between any two regions, such as the volume of tissue incorporated in a volume between the target volume and an outer contour. Results were normalized to 100% of the desired dose to the target volume and to the total volume of the region of interest.

Two other figures of merit were calculated–integral dose and localization factor. The integral dose is the integral of the dose-volume histogram and is calculated for 1 Gy dose to the target, so that the actual integral dose for any particular desired target dose can be calculated easily. The localization factor is the fraction of radiation energy that is delivered to the target volume. It is defined by the ratio of the integral dose of the target volume to the integral dose of the entire brain.

RESULTS

Figure 2 is a dose-volume histogram of a 2 cm diameter (volume = 4 cm^3) spherical target lesion. The histogram is calculated for protons, carbon ions, and 8-MV photons. All three radiation types resulted in nearly identical coverage of the target lesion; the dose is uniform to ± 5% over the entire volume (100% of the volume received ≥90% of the dose). Using these radiation types and the irradiation geometries described above, similar target dose-volume histograms were calculated for the entire range of target volumes, locations, and shapes studied.

Figure 3 shows four dose-volume histograms of the entire brain calculated for four different lesion volumes taken from the series of patients treated at LBL –0.8, 5, 14, and 56 cm^3; the AVMs were taken from the series of patients treated at LBL. The volume of the brain is approximately 1300 cm^3. Each histogram is calculated for protons, helium ions, carbon ions, neon ions, and 8-MV photons, except for the 14 cm^3 lesion which is calculated for carbon ions and photons. The close grouping of the plots for each different charged particle species is common to all of the target volumes studied. Generally, the histograms for helium and carbon ions are slightly beneath those of protons and neon ions. The relative shapes and positions of the charged particle histograms relative to those of the photons is also evident in all target volumes studied. As illustrated in Figure 3, the separation between the two sets of histograms is most pronounced at large volumes, although discernible differences are seen at all volumes.

Table 1 lists the results of calculations for the six lesions chosen from actual cases. The integral doses to the entire brain and the AVM, the localization factors, the treatment volume and location, and the radiation type are shown. The differences in the integral doses for different charged particle species reflect the results described for dose-volume histograms; helium and carbon ions are slightly better than protons and neon ions. This is also reflected in the values of the localization

factors. The relative differences between charged particles and photons also mirror the histogram results. In general, the integral doses for the charged particles are between 2 and 3 times smaller than for photons.

In order to assess the effect of approximating the arc methods with fixed beams and reducing the number of Gamma Knife beamports, dose-volume histograms and integral doses were calculated for the entire brain and a 1 cm thick shell surrounding the target volume for a 2 cm diameter target volume using a range of beamport numbers. Using the Gamma Knife beamport geometry, calculations were performed with 18, 54, 80, 99, and 179 beamports. The results were within a few percent for all except the 18 beamport configuration. The Gamma Knife and Linac irradiation geometries were compared with one another, and the difference in the integral doses and dose-volume histograms were a few percent or less. Therefore, we have grouped both of these geometries under the classification of "photon".

Beamport dose profiles for photons were compared with the published profiles [5,9] for a 2 cm diameter beam, and the shapes were in excellent agreement. One-dimensional dose profiles were calculated for the Linac geometry, and they were compared to published results. Our calculated dose profiles were in good agreement with the reported profiles.

An example of the dose delivered to a defined anatomic structure within the brain is demonstrated by the dose-volume histogram in Figure 4. The target lesion was a 28 cm^3 AVM located in the right caudate and putamen anteriorly and the globus pallidus and thalamus posteriorly. The brainstem and midbrain were contoured on MRI images and the contours were transferred to the CT images using stereotactic image correlation techniques. The target volume did not overlap the contoured brainstem volume. A marked difference exists between the dose-volume histograms for carbon ions and for photons. The integral dose to the structure for the photons is greater by more than a factor of 2 than the integral dose for the

carbon ions.

Figure 5 plots the dose-volume histogram for a 1 cm thick shell surrounding a medium-sized (4.2 cm^3) spherical lesion; the volume of the shell is 29 cm^3. The results are shown for carbon ions and photons. As in Figure 4, a noticeable difference exists between the charged particles and the photons. Histograms were calculated for 1 cm thick shells surrounding spherical targets of 1, 2, 3, 4, and 5 cm diameter for protons and photons. The results are shown in Figure 6, along with the integral doses. The volumes are normalized so that the shapes can be compared; the actual histograms must be scaled by the shell volumes. The proton histograms exhibit relatively small variation in shape as a function of target volume, whereas the photon histograms become progressively flatter on top as target volume increases. The results of such calculations are summarized in Figure 7 for protons, carbon ions, and photons. Since complications may be the result of normal tissue receiving high doses, we have plotted the volume of normal tissue that received 80% or more of the maximum target dose as a function of target size. There is very little difference between protons and carbons, and a very noticeable difference between the charged particles and photons. For all values of the target volume, for photon irradiation the high-dose normal tissue volume is comparable to the target volume.

DISCUSSION

3-Dimensional Calculations

The need to use 3-dimensional calculations to provide quantities that facilitate meaningful comparisons between different techniques is demonstrated with several examples. Figure 8a is a schematic of three different methods of calculating the volume of an irregularly shaped volume; Figure 8b is a plot of the volume of the AVM calculated using two different methods versus the volume calculated using 3-dimensional CT data. Calculations were performed using the last twenty

consecutive cases treated at LBL. The value of the ordinate represents the percent difference between an approximate calculation of the AVM volume and a more exact calculation. One approximate method, represented by solid points, is to idealize the AVM as a parallelopiped by multiplying the length, width and height of the lesion as visualized on angiographic film projections. The exact method calculates volume of the AVM by counting the voxels (.029 cm^3/voxel) that fall within the target contour on each CT slice. The open points represent the AVM volume idealized as an ellipsoid with the projected length, width and height dimensions used as the lengths of the axes. The rectangular method overestimates the volume regardless of true AVM volume as expected. The magnitude of the differences is quite large in many cases and can easily skew comparisons. The ellipsoid method provides a better estimate, but still differs by more than 25% in a number of cases. These two calculations can be characterized as comparable to 1-dimensional dose profiles and 2-dimensional isodose contours, respectively, in the way that the 3-dimensional information is approximated.

These differences in the simplest calculations that would be performed when making comparisons between different treatment centers underscore the need for a standardized, 3-dimensional method of calculation. The incomplete nature of calculations that do not take into account the 3-dimensional aspects are acknowledged in the literature. Podgorsak, et al. [11] state that though dose profiles can be improved in certain directions by changing irradiation techniques, the integral dose is not improved. Dahlin and Sarby[3] present dose profiles along three different axes, all of which differ from one another. As Chen points out [2], 3-dimensional dose-volume histograms are needed in order to provide enough information in order to make meaningful evaluations of treatment plans.

Dose to Target Volume and Brain

An ideal treatment plan covers the entire target volume with a uniform dose,

and each of the histograms calculated approaches that ideal, with nearly the entire lesion receiving within 5% of the desired dose. These results are similar for all of the target volumes examined. The histograms calculated in this work reflect the best possible dose distributions obtainable using each radiation type and the given irradiation geometry. The charged particle treatment plans were calculated for exactly compensated beams on each treatment port and for beam collimating apertures that match the shape of the projected target volume in the beamport direction. In practice, the compensation may not be quite so precise, although there is no difficulty in correctly collimating the beam. The photon treatment plan had no compensation but for all beamports, beam collimating apertures as described above were used. This is not feasible in practice given the large number of beamports or continuous arcs of photon irradiation geometries, except in the case of spherical target volumes.

In determining the dose to normal tissue, the most obvious volume to examine is the remainder of the brain. For normal tissue, the ideal situation is a histogram that falls as close to the coordinate axes as possible. Using the localization factors–the fraction of energy deposited in the target volume–as a figure of merit, some rough comparisons can be made. These conclusions are also born out by examination of the dose-volume histograms. Among the charged particle treatment plans, carbon and helium ions give roughly the same values, as do protons and neon ions. The higher values of the localization factors for carbon and helium reflect the reduced multiple scattering as the projectile mass increases and a lower probability of fragmentation relative to larger mass ions. The similar results for protons and neon ions reflect the improved entrance dose of neon relative to protons due to the sharper Bragg peak, and the inferior exit dose as a result of projectile fragmentation.

Comparing the results of the charged-particle calculations to those of the

photons, one sees that the localization factors are roughly a factor of 2 larger and that the integral doses to the brain are smaller by a factor of 2 to 2.5. The photon treatment plans give a slightly improved integral dose to the AVM due to the large number of beamports which provide complete coverage of the target volume. The differences between different species of charged particles are much smaller than those between any of the charged particles and photons.

Caution must be used in examining these figures. When looking at the localization factors as a function of target volume, one sees that the larger the volume, the larger the fraction of energy deposited within the target volume. However, when one examines the integral doses to the brain, it is clear that treatment of the larger volumes actually results in a substantially greater radiation burden to the brain.

Dose to Circumscribed Regions Outside of Target

The above results for the radiation dose delivered to the entire brain demonstrates the differences between radiation types when one is concerned with the complications and long-term effects resulting from relatively low dose, whole brain irradiations. Complications may also arise from small volumes of tissue receiving large doses of radiation. We have attempted to quantify such effects by two means. The first is to target vital structures which would cause severe complications should radiation injury occur to them. The other is to define shells of normal tissue surrounding the target volume without regard to the radiobiological characteristics or physiological importance. This was done with the idea in mind that given the dose distributions resulting from the treatment planning techniques used, these regions of tissue were the most likely to receive large doses.

The results shown in Figures 4 and 5 demonstrate the substantial difference in the irradiation patterns of charged particles and photons. Examination of the dose delivered to any given structure of interest within the brain is perhaps the most useful calculation for the evaluation of competing treatment plans. The evaluation

of dose to surrounding shells is less specific as far as evaluating possibilities of complications, but it has the advantages that it is an unambiguous and unbiased calculation and that it is most likely to encompass the entire region of high dose. The shell calculations serve to improve the resolution of dose-volume histograms in the high dose region.

We have chosen the shell calculations as the best means to compare results of different radiation types for different target sizes, shapes and locations. Comparisons using particular brain structures suffer from the problem that the results are strongly dependent on the relationship of the target volume to the circumscribed volume. Beamports can be chosen such that the given structure receives minimal radiation, at the expense of another structure which is not being examined. As stated above, these considerations are most appropriate when deciding between competing treatment plans in an individual clinical circumstance.

Dose-volume histograms for various thicknesses of surrounding shells change in shape as the shell thickness varies. For very thin shells, the histograms resemble the histograms for the target volume; as the shells increase in size, the histograms approach the shapes shown above for the entire brain. These changes result from incorporating more of the low dose region as the shell expands away from the target volume. Appropriate sized shells can be chosen to encompass the desired region of interest for a given comparison.

Effects of Target Size

Of all of the variables studied, the effects on the dose-volume histograms were most pronounced as the size of the target was varied. Target volumes ranged from 0.5 to 65 cm^3. The relative positions of the dose-volume histograms for each radiation type studied remained the same for all volumes, as shown in Figure 3. Figures 6a and 6b illustrate the differences in histogram shape between charged particles and photons as a function of target volume. Using spherical targets, these

plots measure the effect of the size of the target volume on the dose distributions in a 1 cm thick shell surrounding the target. The histogram shapes do not change markedly for protons as the target volume increases; the photon histograms become progressively worse as the target volume increases. This difference reflects the overlapping of adjacent and nearly opposed photon beams, whereas the Bragg peak and compensation of the particle beams remain relatively the same, even as beam size increases.

Figure 7, using a figure of merit–the volume of normal tissue that receives 80% or more of the target dose–, summarizes the results for several radiation types and a wide range of target volumes. For the charged particles, the volume of normal tissue irradiated to 80% is roughly 1/3 of the volume of the target; for photons it is approximately equal. At small volumes, although the charged particles result in less normal tissue irradation, the absolute volume is small for both types of radiation. As the target volume increases, the absolute magnitude of the volume of normal tissue receiving a relatively high dose increases significantly.

Effects of Target Volume Shape and Location

In this limited sample of AVM targets, there existed a range of target shapes and locations. No attempt was made to pick shapes that might systematically measure the effect of target volume irregularity on the dose-volume histograms. AVM locations were chosen to cover the range of centrally located lesions to those located adjacent to the skull. No significant differences between spherical targets and the irregularly-shaped volumes were noted for targets of roughly the same volume. Given the ability to provide compensation, to adjust the width of the spread-out Bragg peak, and to match the beam aperture to the target shape for charged particles, this was not a surprising result. The photon results are the best possible owing to the use of shaped beam port apertures in the treatment planning calculations. This is not the clinically-realized situation, and work is continuing to

model that aspect and to calculate the results.

The location of the target volume did have a small effect on the results for charged particles. This is due to the choice of beamports and the nature of the Bragg peak. Whenever the target volume did not lie on the midline, all beamports were chosen to enter from the side of the head in which the target was located. For peripheral lesions, this means that each beam traverses only a short segment of normal tissue. The Bragg peak of charged particles results in no (or very small) dose distal to the end of the particle range except for that due to fragments of the primary ions. A more systematic study of this needs to be accomplished.

For photons, there was little dependence in the histograms and integral doses on the target location. This is a result of the bilateral arrangement of beamports and the exponential depth dose characteristic of photon radiation.

Effects of Irradiation Geometries

The effects of irradiation geometries of several different systems was investigated. Very small differences were found between the Linac geometry and the Gamma Knife geometry. We would like to emphasize that our results in this regard are incomplete owing to limitations in our current treatment planning program (such as the automatic determination of the beamport aperture shapes), and the lack of clinical treatment planning input for each particular case using these modalities. Work is proceeding to incorporate these factors so that comparisons between different photon modalities can be made.

The effect of beamport number was investigated for charged particles and photons. Although no attempt was made to discover the optimal number of beamports for charged particles, only small differences were seen for the beamport selection described above and for the case in which the beamport geometry of the Linac method was applied using carbon ion beams. The number of beamports was varied from 54 to 179 beams for the photon methods (both Linac and Gamma Knife ge-

ometries) and only very small differences were seen. Integral doses and localization factors differed by 2% or less over the range of beamport number investigated.

SUMMARY

3-dimensional calculations are fundamental to meaningful comparisons of different modalities in stereotactic radiosurgery. This is particularly important as a result of the multi-directional nature of the beamports used. Dose-volume histograms, integral doses, and localization factors are useful in quantitating the dose distributions and evaluating their effects. These methods were applied to several radiation types and irradiation geometries currently used in the stereotactic radiosurgical treatment of intracranial lesions. A range of charged particle species was investigated, as well as photons. Three different irradiation geometries were selected. Other variables investigated included the size, shape and location of the treatment volume, and various designated regions of normal tissue. In each case, it was found that each species of charged particle produced dose distributions that were roughly comparable, but with slightly better results for carbon and helium ions when compared to protons and neon ions. It was also found that the photon dose distributions were worse than for ions for all situations studied. The differences are quite small for small target volumes, but become markedly larger as target volume increases. Of all of the variables studied, target volume had the greatest effect on comparisons between charged particles and photons. More work is needed to more accurately calculate dose distributions for photon radiosurgical techniques. We hope that this work will help evaluate different techniques and methods, and that it can be used to establish the relationships between physical dose distributions and clinical results–both successes and complications.

Bibliography

[1] Barcia-Salorio, J.L.; Hernandez, G.; Brosta, J.; Ballester, B.; Masbout, G. Radiosurgical treatment of a carotid-cavernous fistula. Case Report. In Szikla, G., editor, *Stereotactic Cerebral Irradiation, INSERM Symposium No. 12*, pages 251–256, Elsevier/North-Holland Press, 1979.

[2] Chen, G.T.Y. Dose volume histograms in treatment planning. *Int J Radiat Oncol Biol Phys*, 14: 1319–1320, 1988.

[3] Dahlin, H.; Sarby, B. Destruction of small intracranial tumours with ^{60}Co gamma radiation: physical and technical considerations. *Acta Radiologica*, 14:209–227, 1975.

[4] Fabrikant. J.I.; Lyman, J.T.; Hosobuchi, Y. Stereotactic heavy-ion Bragg peak radiosurgery: method for treatment of deep arteriovenous malformations. *Br J Radiol*, 57:479–490, 1984.

[5] Hartmann, G.H.; Schlegel, W.; Sturm,V.; Kober, B.; Pastyr, O.; Lorenz, W.J. Cerebral radiation surgery using moving field irradiation at a linear accelerator facility. *Int J Radiat Oncol Biol Phys*, 11:1185–1192, 1985.

[6] Kjellberg, R.N.; Hanamura, T.; Davis, K.R.; Lyons, S.L.; Adams, R.D.. Bragg peak proton-beam therapy for arteriovenous malformations of the brain. *N Engl J Med*, 309:269–274, 1983.

[7] Lawrence, J.H. Heavy particle irradiation of intracranial lesions. In Wilkins,

R.H. and Rengcharry, S.S., editors, *Neurosurgery*, page 1113, McGraw-Hill, Philadelphia, 1985.

[8] Levy, R.P.; Fabrikant, J.I.; Frankel, K.A.; Phillips, M.H.; Lyman, J.T. Stereotactic heavy-charged-particle Bragg peak radiosurgery for the treatment of intracranial arteriovenous malformations in childhood and adolescence. Submitted to *Neurosurgery*, 1988.

[9] Lutz, W.; Winston, K.R.; Maleki, N. A system for stereotactic radiosurgery with a linear accelerator. *Int J Radiat Oncol Biol Phys*, 14:387-381, 1988.

[10] Lyman, J.T.; Fabrikant, J.I.; Frankel, K.A.. Charged particle stereotactic radiosurgery. *Nuclear Instruments and Methods in Physics Research*, B10/11:1107–1110, 1985.

[11] Podgorsak, E.B.; Olivier, A.; Pla, M.; Lefebvre, P.Y.; Hazel, J.. Dynamic stereotactic radiosurgery. *Int J Radiat Oncol Biol Phys*, 14:115–126, 1988.

[12] Steiner, L. Treatment of arteriovenous malformations by radiosurgery. In Wilson, C.B. and Stein, B.M., editors, *Intracranial Arteriovenous Malformations*, pages 295–313, Williams and Wilkins, Baltimore, 1984.

[13] Sturm, V.; Kober. B.; Höver, K.H.; Schlegel, W.; Boesecke, R.; Pastyr, O.; Hartmann, G.H.; Schabbert, S.; zum Winkel, K.; Kunze, S.; Lorenz, W.J. Stereotactic percutaneous single dose irradiation of brain metastases with a linear accelerator. *Int J Radiat Oncol Biol Phys*, 13:279–282, 1987.

FIGURE CAPTIONS

Figure 1: Depth dose curves for different radiation types. The depth dose curves for the following charged particle species are shown: protons (150 MeV, 2 cm spread Bragg peak), helium ions (150 MeV/amu, 2 cm spread Bragg peak), carbon ions (285 MeV/amu, 2 cm spread Bragg peak), and neon ions (456 MeV/amu, 2 cm spread Bragg peak). These are isoeffect curves–the physical dose has been modified by an LET-dependent RBE. Also shown is the depth dose curve for a 10x10 cm field of 8 MV linear accelerator-produced photons. All curves have been normalized to 1 at their peak dose. The curves are for absorption in water.

Figure 2: Dose-volume histograms calculated for a 2 cm diameter spherical target located in the center of the brain. Histograms are calculated for protons, carbon ions, and photons. The ordinate has been scaled to a total volume of 1; the actual volume is 4.2 cm^3.

Figure 3: Dose-volume histograms calculated for the entire brain (volume = 1300 cm^3) for four different sizes of target volumes. The target volumes are 0.8, 5.0, 14, and 56 cm^3. The histograms are shown for protons, helium ions, carbon ion, neon ions, and photons except for the 14 cm^3 target where only results for carbon ions and photons are presented.

Figure 4: Dose-volume histograms calculated for the brainstem. The target volume was a 28 cm^3 lesion located in the right caudate and putamen anteriorly and the globus pallidus and thalamus posteriorly. The target volume and the contoured volume did not overlap. The brainstem was contoured on MRI images and the contours were transferred to the CT images using stereotactic image correlation techniques. Histograms were calculated for carbon ions and photons.

Figure 5: Dose-volume histograms calculated for a 1 cm thick shell surrounding a 2 cm diameter spherical target volume. The volume of the shell was 29 cm^3 and the volume of the target was 4.2 cm^3. Histograms were calculated for

carbon ions and photons. The integral doses were 9 cm^3/Gy for carbon ions and 14 cm^3/Gy for photons.

Figure 6: Dose-volume histograms for 1 cm thick shells surrounding spherical target lesions of 1, 2, 3, 4, and 5 cm diameter. (a) Dose-volume histograms calculated for protons. (b) Dose-volume histograms calculated for photons. The histograms have all been scaled to a total volume of 1. The actual volumes for the 1, 2, 3, 4, and 5 cm diameter volumes are 0.5, 4.2, 14, 33, and 65 cm^3, respectively. The integral doses, in units of cm^3/Gy, are presented in the upper right of the figures.

Figure 7: This figure plots the volume of tissue outside of the target volume that received 80% or more of the dose delivered to the target as a function of target volume. The results are plotted for protons, carbon ions, and photons.

Figure 8: (a) Schematic representations of an irregularly-shaped 3-dimensional volume and three methods for calculating its volume. The upper right panel shows the relationship between the volume and a rectangular parallelopiped with dimensions corresponding to the projected length, width and height of the irregular volume. The lower left panel shows its relationship to an ellipsoid with axes corresponding to the projected dimensions. The lower right panel shows the volume as being made up of a large number of small cubic voxels. (b) The percent difference between the volumes of 20 different AVMs calculated by the rectangular method (solid squares) and the ellipsoidal method (open squares) and the volumes calculated using the voxel method is plotted against the AVM volume calculated using the voxel method. The deviation of the points from the 0% difference axis illustrates the errors that can occur if 3-dimensional calculations are not performed for dose comparisons.

TABLE CAPTIONS

Table 1: The integral doses to the brain and the target volume, i.e. the AVM) and the localization factors are given for six different AVMs chosen from LBL patient files in order to span a range of target sizes and locations. The results are presented for five different radiation types–protons, helium ions, carbon ions, neon ions, and 8 MV photons.

VOLUME (cm^3)	LOCATION	BEAM ion, MeV/amu	ID (Brain)[a] (cm^3·Gy)	ID (AVM)[b] (cm^3·Gy)	Localization Factor[c]
0.8	center	H, 150	26	0.34	.013
		He, 150	27	0.44	.016
		C, 285	18	0.36	.020
		Ne, 456	22	0.35	.016
		Photons, 8 MV	37	0.35	.0094
1.6	periphery	H, 150	16	0.89	.057
		He, 150	15	1.2	.078
		C, 285	13	0.88	.070
		Ne, 456	15	0.90	.061
		Photons, 8 MV	31	0.98	.032
5.0	center	H, 150	46	4.8	.10
		He, 150	39	4.9	.13
		C, 285	33	4.8	.15
		Ne, 456	42	4.8	.11
		Photons, 8 MV	82	5.0	.061
5.7	periphery	H, 150	28	3.8	.14
		He, 150	25	4.0	.16
		C, 285	24	3.8	.16
		Ne, 456	29	3.9	.13
		Photons, 8 MV	64	4.0	.062
28	center	H, 150	133	28	.21
		He, 150	147	33	.22
		C, 285	106	27	.26
		Ne, 456	130	27	.21
		Photons, 8 MV	213	28	.13
56	periphery	H, 150	144	55	.38
		He, 150	124	49	.40
		C, 285	129	54	.42
		Ne, 456	145	54	.38
		Photons, 8 MV	292	57	.20

[a]Integral Dose for 1 Gy target dose
[b]Integral Dose for 1 Gy target dose
[c]LF = ID(AVM)/ID(Brain)

TABLE 1

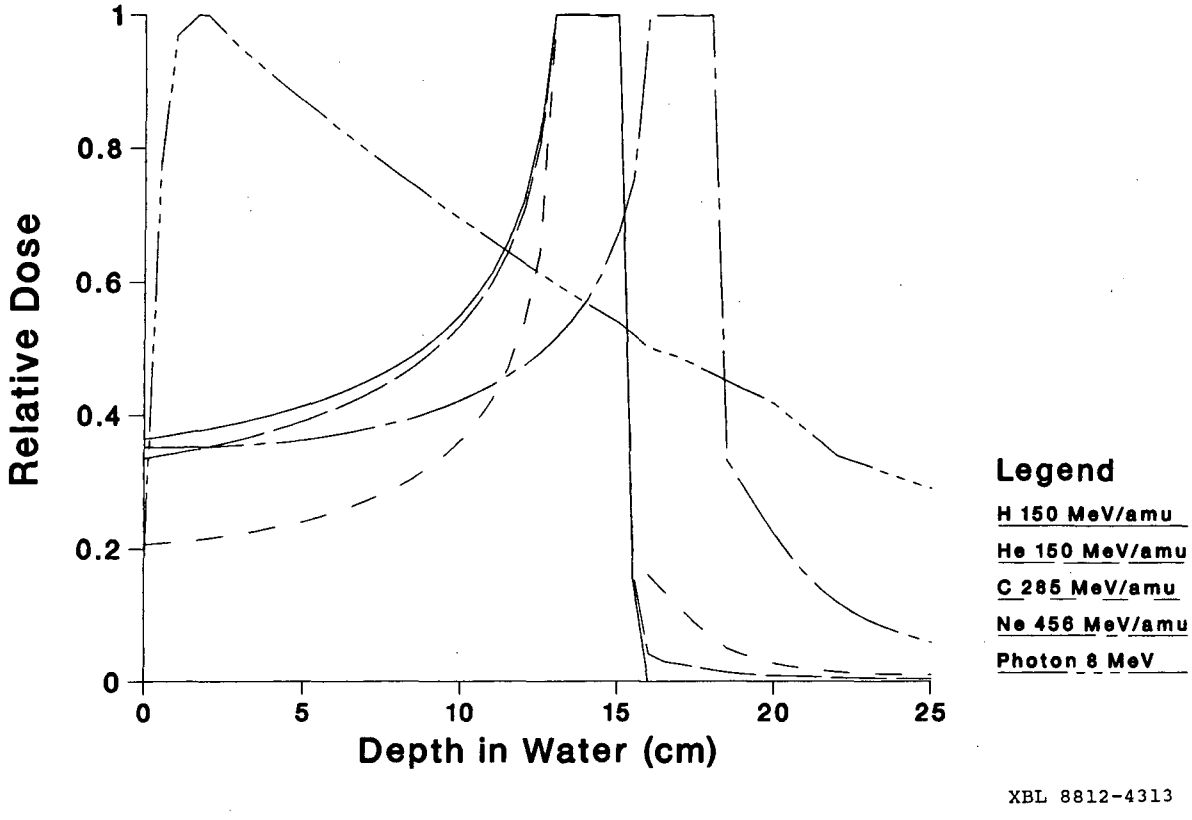
Relative Dose
1
0.8
0.6
0.4
0.2
0
0
5
10
15
20
25
Depth in Water (cm)
Legend
H 150 MeV/amu
He 150 MeV/amu
C 285 MeV/amu
Ne 456 MeV/amu
Photon 8 MeV
XBL 8812-4313

Figure 1

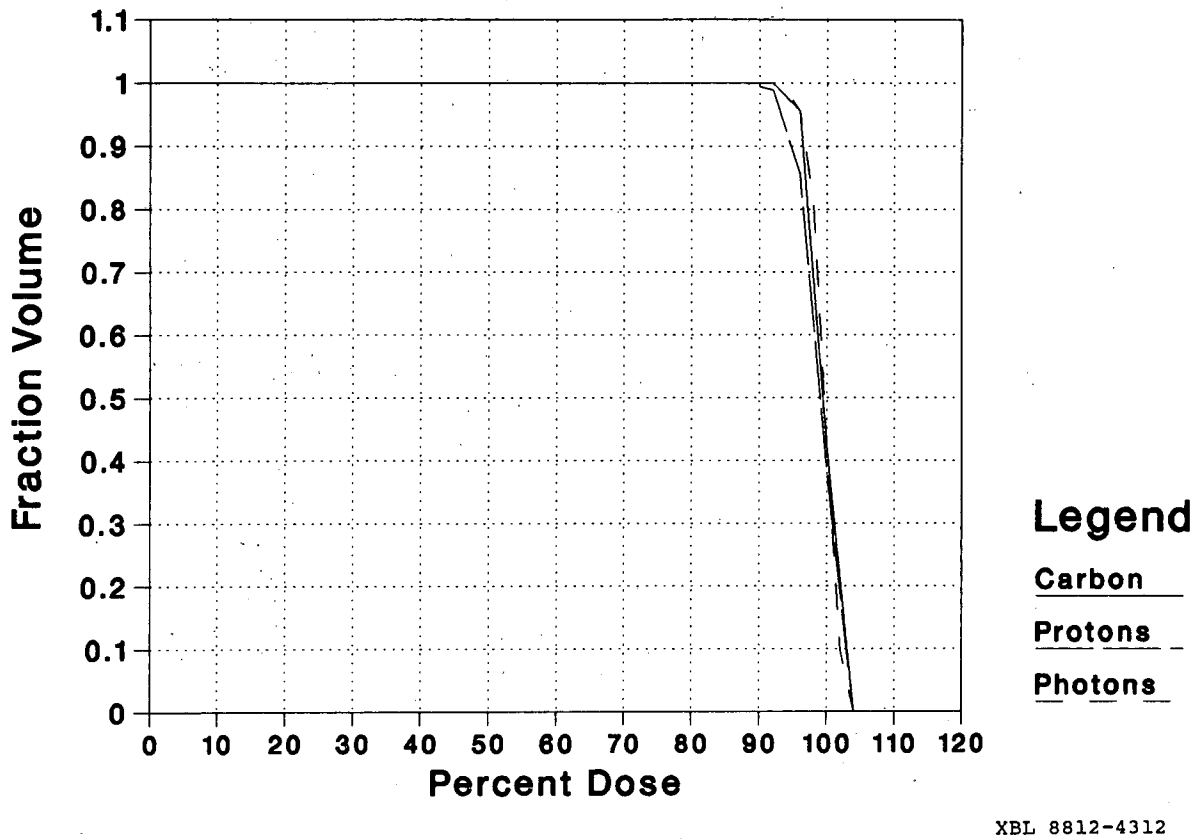
1.1
1
0.9
0.8
0.7
0.6
0.5
0.4
0.3
0.2
0.1
0
Fraction Volume
0 10 20 30 40 50 60 70 80 90 100 110 120
Percent Dose
Legend
Carbon
Protons
Photons
XBL 8812-4312

Figure 2

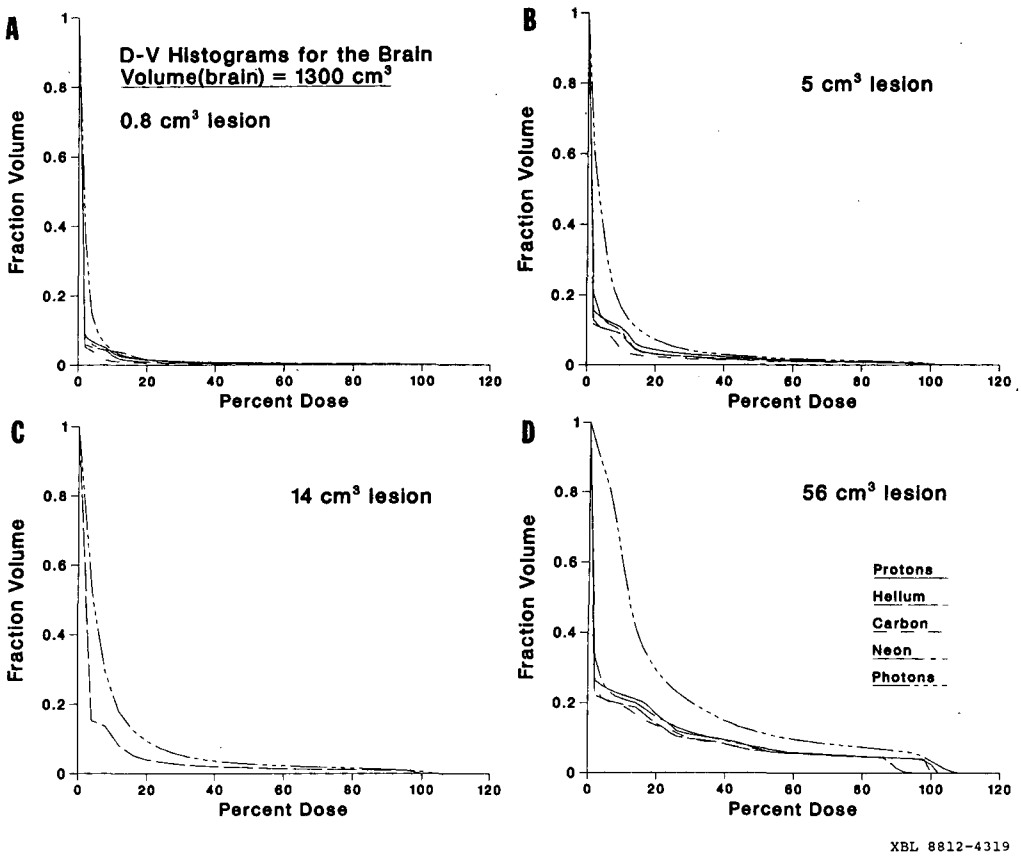
A
D-V Histograms for the Brain
Volume(brain) = 1300 cm³
0.8 cm³ lesion
B
5 cm³ lesion
C
14 cm³ lesion
D
56 cm³ lesion
Protons
Helium
Carbon
Neon
Photons
Fraction Volume
Percent Dose
XBL 8812-4319

Figure 3

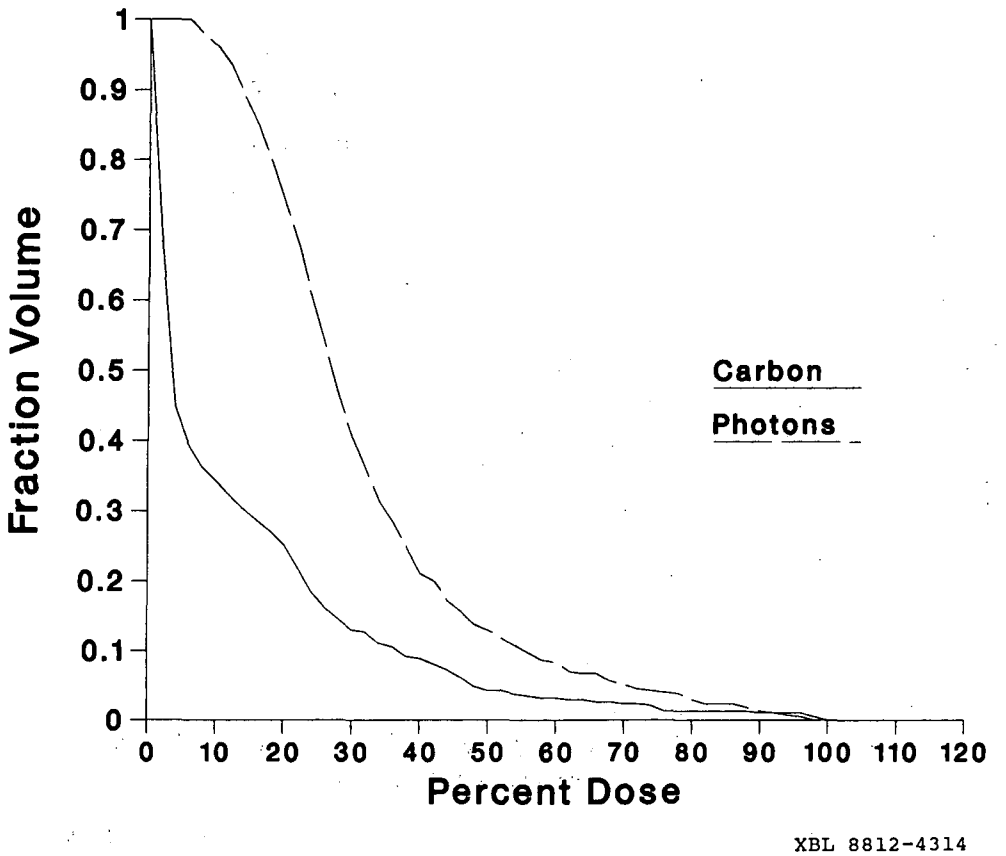
Fraction Volume
1
0.9
0.8
0.7
0.6
0.5
0.4
0.3
0.2
0.1
0
0 10 20 30 40 50 60 70 80 90 100 110 120
Percent Dose
Carbon
Photons
XBL 8812-4314

Figure 4

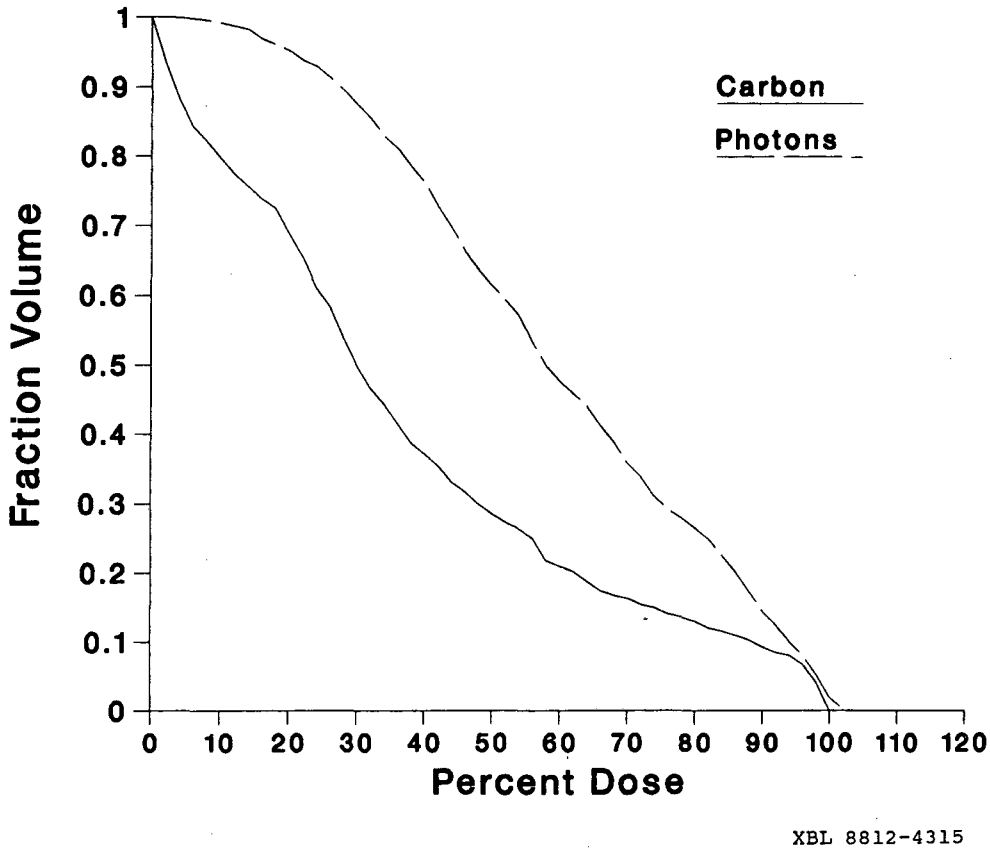
Fraction Volume
1
0.9
0.8
0.7
0.6
0.5
0.4
0.3
0.2
0.1
0
0 10 20 30 40 50 60 70 80 90 100 110 120
Percent Dose
Carbon
Photons
XBL 8812-4315

Figure 5

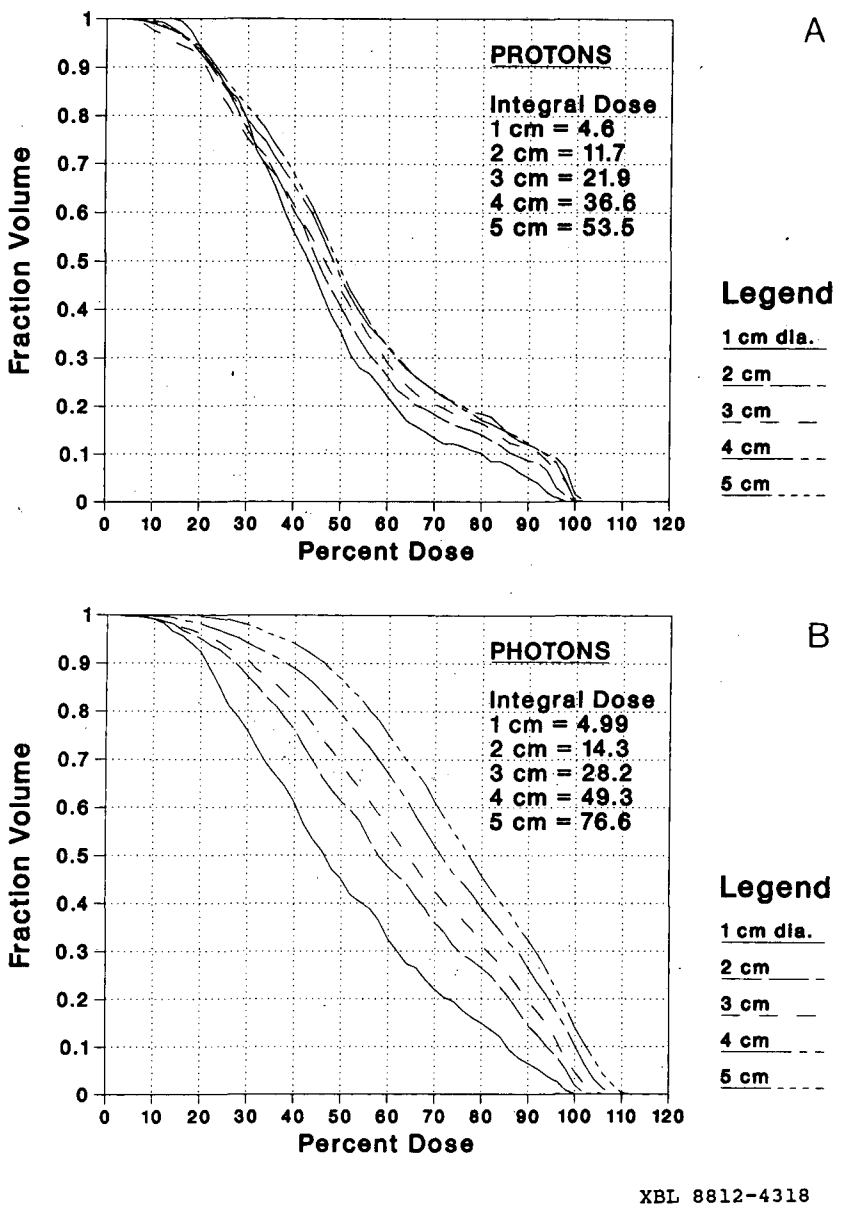
A
PROTONS
Integral Dose
1 cm = 4.6
2 cm = 11.7
3 cm = 21.9
4 cm = 36.6
5 cm = 53.5
Fraction Volume
Percent Dose
Legend
1 cm dia.
2 cm
3 cm
4 cm
5 cm
B
PHOTONS
Integral Dose
1 cm = 4.99
2 cm = 14.3
3 cm = 28.2
4 cm = 49.3
5 cm = 76.6
Fraction Volume
Percent Dose
Legend
1 cm dia.
2 cm
3 cm
4 cm
5 cm
XBL 8812-4318

Figure 6

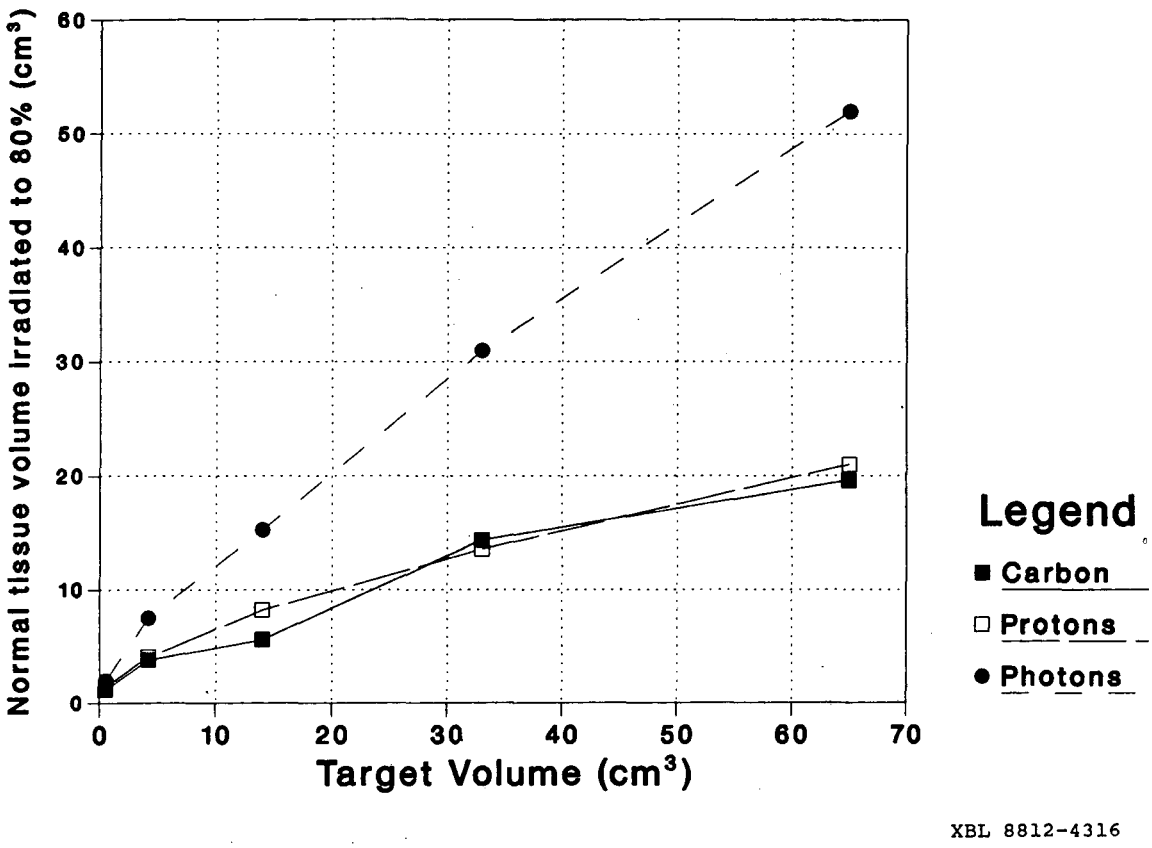
Normal tissue volume irradiated to 80% (cm³)
Target Volume (cm³)
0
10
20
30
40
50
60
70
Legend
Carbon
Protons
Photons
XBL 8812-4316

Figure 7

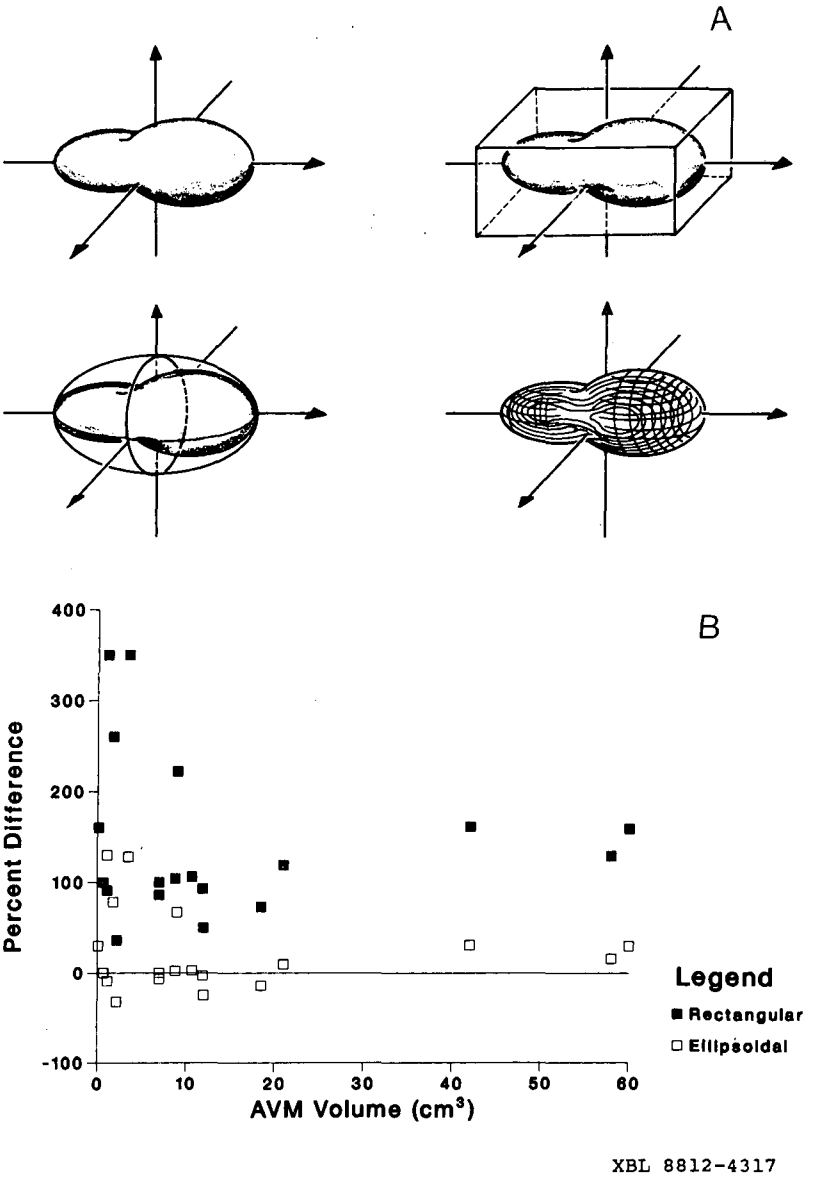
A
B
Percent Difference
400
300
200
100
0
-100
0
10
20
30
40
50
60
AVM Volume (cm³)
Legend
Rectangular
Ellipsoidal
XBL 8812-4317

Figure 8

LAWRENCE BERKELEY LABORATORY
TECHNICAL INFORMATION DEPARTMENT
1 CYCLOTRON ROAD
BERKELEY, CALIFORNIA 94720